Short-wave directional properties in the vicinity of atmospheric and oceanic fronts

Yukiharu Hisaki

Department of Physics and Earth Sciences, Faculty of Science, University of the Ryukyus, Okinawa, Japan

Received 9 April 2001; revised 20 May 2002; accepted 30 May 2002; published 13 November 2002.

[1] The author estimated and investigated mean wave directions and directional spread parameters of 0.505 Hz ocean waves using data from 24.5 MHz-HF ocean radar. The author described temporal and spatial variabilities of the short-wave field. The short-wave direction is a good indication of wind direction. The spread parameter was related to the variability of wind direction. The author examined the case that an atmospheric front or an oceanic front exists in the HF ocean radar observation area. In the case of an atmospheric front the short-wave direction changed with the passage of the atmospheric front. Furthermore, the complicated frontal structure, which cannot be verified from a weather chart, was revealed. Narrow directional spread was observed in the vicinity of the convergent front, which was reproduced using a simplified model based on the wave action conservation law. The result shows that wave refraction associated with a frontal convergent zone is important in determining the spatial variability of short-wave directional properties. *INDEX TERMS:* 4275 Oceanography: General: Remote sensing and electromagnetic processes (0689); 4504 Oceanography: Physical: Air/sea interactions (0312); 4560 Oceanography: Physical: Surface waves and tides (1255); *KEYWORDS:* HF radar, short-wave direction, front, spread parameter, Bragg scattering

Citation: Hisaki, Y., Short-wave directional properties in the vicinity of atmospheric and oceanic fronts, *J. Geophys. Res.*, *107*(C11), 3188, doi:10.1029/2001JC000912, 2002.

1. Introduction

[2] It is important to measure ocean surface currents and surface waves for physical oceanography and engineering applications. One promising method of effectively measuring spatially evolving current and wave fields is to use HF (high-frequency) ocean radar. HF ocean radar is used to measure ocean surface currents and waves by radiating high-frequency radio waves and analyzing backscattered signals from the ocean. The power spectrum (called the Doppler spectrum) of backscattered signals is characterized by two peaks, i.e., it is a first-order spectrum. The two first-order Bragg peaks are associated with radio wave backscatter from ocean waves with half the radio wavelength moving directly toward, for a peak at positive frequency, or away from, for a negative peak, the radar site. This scattering is Bragg scattering. The wave components contributing to Bragg scattering are called the Bragg waves, and the frequency of the Bragg waves is called Bragg frequency. Furthermore, the two first-order Bragg peaks are surrounded by the second-order continuum, which is called second-order scattering. All of the wave components contribute to second-order scattering.

[3] With regard to ocean surface waves, HF ocean radar can be used to measure wave heights [e.g., *Barrick*, 1977], dominant wave periods [e.g., *Forget et al.*, 1981], and wave directional spectra [e.g., *Hisaki*, 1996] from first- and second-order scattering. On the other hand, short-wave directional properties [e.g., *Heron*, 1987; *Wyatt et al.*, 1997] are estimated from first-order scattering. The short-wave direction is an indication of wind direction [e.g., *Harlan and Georges*, 1994].

[4] In general, measurement of the wave directional spectrum requires a good signal-to-noise ratio in the Doppler spectrum but such a region is quite limited. For most HF radar observations, the signal-to-noise ratio was sufficient to identify the first-order scattering from which short-wave directional properties could be estimated over most of the region of radar coverage.

[5] Short-wave directional properties and surface currents estimated with fine spatial resolution provide information on the dynamics of waves and currents. For example, when ocean waves propagate through a spatially varying current, their properties can be significantly affected. The influence of surface currents on ocean waves has been known, but detailed quantitative measurements of this phenomenon are scarce. Some studies on wave-current interaction have been based on measured current and wave data [e.g., *Wang et al.*, 1994; *Masson*, 1996], however, there are no studies on the measurement of both surface currents and ocean waves with a fine resolution.

[6] This study had three main objectives. The first was to describe short-wave directional properties with a fine resolution. The second was to describe the short-wave directions associated with the passage of an atmospheric front. The

0148-0227/02/2001JC000912$09.00

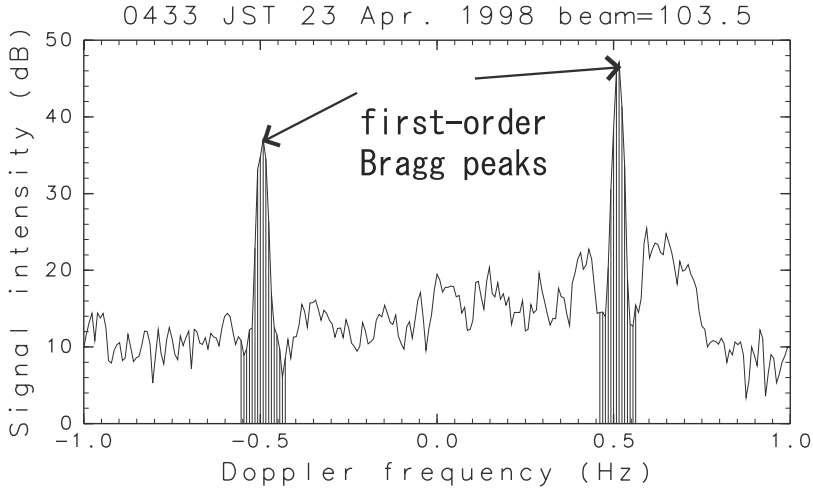

Figure 1. Example of a Doppler spectrum.

third was to investigate wave-current interaction with a fine resolution.

[7] The HF ocean radars of Okinawa Radio Observatory (Okinawa Subtropical Environment Remote-Sensing Center), Communications Research Laboratory, were deployed along the coast of the eastern part of Okinawa Island, Japan from 15 April 1998 to 15 May 1998. A strong convergent zone associated with mesoscale eddies were found on 17 April 1998 [*Hisaki et al.*, 2001]. The author investigated short-wave directional properties during this period. Furthermore, an atmospheric front passed over the HF radar observation area during the HF radar observation period. The author also investigated short-wave properties in response to wind direction changes associated with the passage of the atmospheric front.

[8] In section 2, the author describes the method of estimating short-wave properties, error analysis due to sampling variabilities of Doppler spectra, and the experimental design. Section 3 presents some results and general features of observed data. The case study of the passage of an atmospheric front is described in section 4. The case of an oceanic front is described in section 5. The conclusions are summarized in section 6. The higher-order effect [*Hisaki*, 1999] and the effect of the finite illuminated area [*Hisaki and Tokuda*, 2001] are not considered in this study.

2. Observation

2.1. Principle of Measuring Ocean Currents Using HF Ocean Radar

[9] The first-order peaks in the Doppler spectrum for deep water are given by

$$\sigma_1(\omega_D) = 2^6 \pi k_0^4 \sum_{m=\pm 1} S(2m\mathbf{k}_0)\delta(\omega_D - m\omega_B), \qquad (1)$$

where $\mathbf{k}_0$ is the incident radio wave number vector, $k_0 = |\mathbf{k}_0|$, ω_D is the radian Doppler frequency, $\omega_B = (2gk_0)^{1/2}$ is the radian Bragg frequency, g is the acceleration of gravity, and $S(\mathbf{k})$ is the wave spectrum composed of free waves for wave number vector $\mathbf{k} = (k \cos\theta, k \sin\theta)$ [e.g., *Barrick*, 1972]. The integral of the Doppler spectrum under the first-order peaks is denoted by σ_- for negative Doppler frequencies and σ_+ for positive Doppler frequencies.

[10] If we write $S(\mathbf{k})$ in terms of k and θ, that is, $S(\mathbf{k}) = S_d(k, \theta)$, for two radars, the ratio of the first-order peaks r_i for radar i (i = 1, 2) is written as

$$r_i \equiv \frac{\sigma_+}{\sigma_-} = \frac{S_d(2k_0, \phi_i + \pi)}{S_d(2k_0, \phi_i)}, \qquad (2)$$

where ϕ_i is the radar beam direction for radar i (i = 1, 2). Furthermore, if we assume that

$$S_d(2k_0, \theta) \propto \cos^{2s}\left(\frac{\theta - \theta_m}{2}\right), \qquad (3)$$

where s is a spread parameter (s value) and θ_m is the mean wave direction for the Bragg wave number, equation (2) is rewritten as

$$r_i = f_i(\theta_m, s) = \tan^{2s}\left(\frac{\phi_i - \theta_m}{2}\right). \qquad (4)$$

Thus, we can estimate θ_m and s from two radar measurements. The estimated short-wave directional properties are mean direction and spread parameter at the Bragg frequency.

[11] The first-order peaks are spread over a finite Doppler frequency band by horizontal current shear, and system and signal processing effects. An integral taken over this finite Doppler frequency band is required to estimate σ_+ and σ_-. The Doppler frequency band has been determined by identifying local minima around the two first-order peaks and integrating between these minima.

[12] Figure 1 shows an example of a Doppler spectrum from the HF ocean radar. The shaded areas in Figure 1 are integrated areas for estimating σ_- and σ_+.

[13] Sometimes first-order Bragg peaks are split due to current variability. In this case, it is reasonable to select the Doppler frequency band for estimating σ_- or σ_+ so as to

include both split peaks. In fact, if there is current variability, equation (1) is rewritten as

$$\sigma_1(\omega_D) = 2^6\pi k_0^4 \sum_{m=\pm 1} \int\int P(x,y)S(-2m\mathbf{k}_0) \cdot \delta(\omega_D - m\omega_B + 2k_0 v_r)dxdy, \quad (5)$$

where $v_r = v_r(x, y)$ is the radial velocity, $P(x, y)$ is the beam pattern for the horizontal coordinate $\mathbf{x} = (x, y)$ and $\int\int P(x, y)dxdy = 1$. Hence,

$$\sigma_-(\text{or } \sigma_+) = \int_{\omega_{ml}}^{\omega_{mu}} \sigma_1(\omega_D)d\omega_D = 2^6\pi k_0^4 S(-2m\mathbf{k}_0), \quad (6)$$

where ω_{ml} and ω_{mu} ($m = \pm 1$) are, respectively, lower and upper radian Doppler frequencies for the first-order scattering. The author identified local minima from running-averaged Doppler spectra to determine ω_{ml} and ω_{mu}.

2.2. Error Estimation

[14] The author has estimated the sensitivities of calculated s and θ_m to sampling variability of measured Doppler spectra. *Barrick* [1980] has shown that the Bragg ratio varies according to the F distribution. That is, the ratio $z_i = r_i/r_{it}$, where r_i is the measured Bragg ratio and r_{it} is the true Bragg ratio for radar i ($i = 1, 2$), obeys the probability density function $pdf(z_i)$ expressed as

$$pdf(z_i) = \frac{\Gamma(\nu)z_i^{(\nu/2)-1}}{\left[\Gamma\left(\frac{\nu}{2}\right)\right]^2(1+z_i)^\nu}, \quad (7)$$

where Γ is the Gamma function and ν is the degrees of freedom determined from signal processing of Doppler spectra. The variance of z_i is written as

$$\sigma_z^2 = \frac{4\nu(\nu-1)}{(\nu-2)^2(\nu-4)}. \quad (8)$$

The ratio z_i is written as

$$z_i = \frac{f_i(\theta_{mt} + \Delta\theta_m, s_t + \Delta s)}{f_i(\theta_{mt}, s_{mt})} \simeq 1 + \frac{\partial \log(f_i(\theta_{me}, s_e))}{\partial\theta_{me}}\Delta\theta_m + \frac{\partial \log(f_i(\theta_{me}, s_e))}{\partial s_e}\Delta s, \quad (9)$$

where θ_{mt} and s_{mt} are, respectively, true values of θ_m and s, $\Delta\theta_m$ and Δs are, respectively, errors of θ_m and s due to sampling variability, and $\theta_{me} = \theta_{mt} + \Delta\theta_m$ and $s_e = s_t + \Delta s$ are, respectively, estimated θ_m and s. Therefore, variances of $\Delta\theta_m$ and Δs are respectively written as

$$\langle\Delta\theta_m^2\rangle = \left[\left(\mathbf{J}_{11}^{-1}\right)^2 + \left(\mathbf{J}_{12}^{-1}\right)^2\right]\sigma_z^2 \quad (10)$$

$$\langle\Delta s^2\rangle = \left[\left(\mathbf{J}_{21}^{-1}\right)^2 + \left(\mathbf{J}_{22}^{-1}\right)^2\right]\sigma_z^2, \quad (11)$$

where $\mathbf{J}_{ij}$ ($i, j = 1, 2$) is the (i, j) component of the matrix defined as

$$\mathbf{J}_{ij} = \left(\frac{\partial \log(f_i)}{\partial x_j}\right), \quad (12)$$

$x_1 = \theta_{me}$ and $x_2 = s_e$. Furthermore, $\mathbf{J}_{ij}^{-1}$ is the (i, j) component of the inverse matrix of $\mathbf{J}$ whose component is defined in equation (12). Thus we can calculate the variances of $\Delta\theta_m$ and Δs from equations (10), (11), (12), (8), and (4) for a given ν.

2.3. Experimental Design and Data Analysis

[15] The HF ocean radars of Okinawa Radio Observatory, Communications Research Laboratory, were deployed along the coast of the eastern part of Okinawa Island. The observation of ocean current fields using these HF ocean radars was conducted from 15 April 1998 to 15 May 1998. The radio frequency was 24.5 MHz, and the Bragg frequency $f_B = \omega_B/(2\pi)$ was 0.505 Hz. The temporal resolution of the radar system was 2 hours.

[16] A map of the observation is shown in Figure 2. The radars were located at site A (26° 7.19′N, 127° 45.78′E) and site B (26°18.63′N, 127°50.25′E). The details of the observation and the radar system have been described by *Hisaki et al.* [2001].

[17] The radar measures one direction in one measurement and changes its direction in the next measurement. We used 12 beam directions in this observation. The radar systems are available as 896 coherent I and Q signals at 0.5 s sampling intervals, and are processed using 256-point fast Fourier transform (FFT) after applying a Hamming window and overlapping by 50 percent. These acquisition parameters are sufficient to resolve the Bragg wave shown in Figure 1. The radar data collection to obtain a Doppler spectrum requires more than $0.5 \times 896 = 448$ s, where each measurement takes 10 minutes per direction. In this signal processing, the degree of freedom of a Doppler spectrum is $\nu_1 = 11$ [*Hisaki*, 1999]. Furthermore, the degree of freedom of integrated first-order Doppler spectra is $\nu = 1.3M_h\nu_1$, where M_h is the number of points within Bragg echo regions, where the spectral values are greater than half the maximum Bragg peak level [*Barrick*, 1980]. Here $M_h = 7$ and $\nu = 100$ were used in equation (8).

[18] The radial component of current along the direction of the radar was estimated by extracting first-order Bragg peaks. There may be cases in which Doppler peaks are due to artificial signals, so the Doppler spectra were manually checked. If there were no significant first-order Bragg peaks in a Doppler spectrum, the Doppler spectrum was deemed not useful and the data was removed. The HF radar system mapped coastal ocean currents, mean wave directions θ_m, and spread parameters s at wave number $2k_0$ with a horizontal resolution of 1.5 km at approximately 450 grid points.

2.4. In Situ Observational Data

[19] Figure 2 also indicates in situ observational points. The surface wind data at 10 min intervals at locations I (Itokazu, 26° 09′N, 127° 46′E, elevation: 186 m), Ng (Nago, 26° 35′N, 127° 58′E, elevation: 6 m), Kn (Kin, 26° 27′N, 127° 51′E, elevation: 8 m), Nh (Naha, 26°12′N, 127° 41′E, elevation: 28 m), and on South-Daito island (25° 49.7′N, 131° 13.5′E, elevation: 14 m) were supplied by the Japan Meteorological Agency (JMA). The 10 min wind at a certain time means a 10 min averaged wind before that time. For example, a wind at 1200 JST (Japan Standard

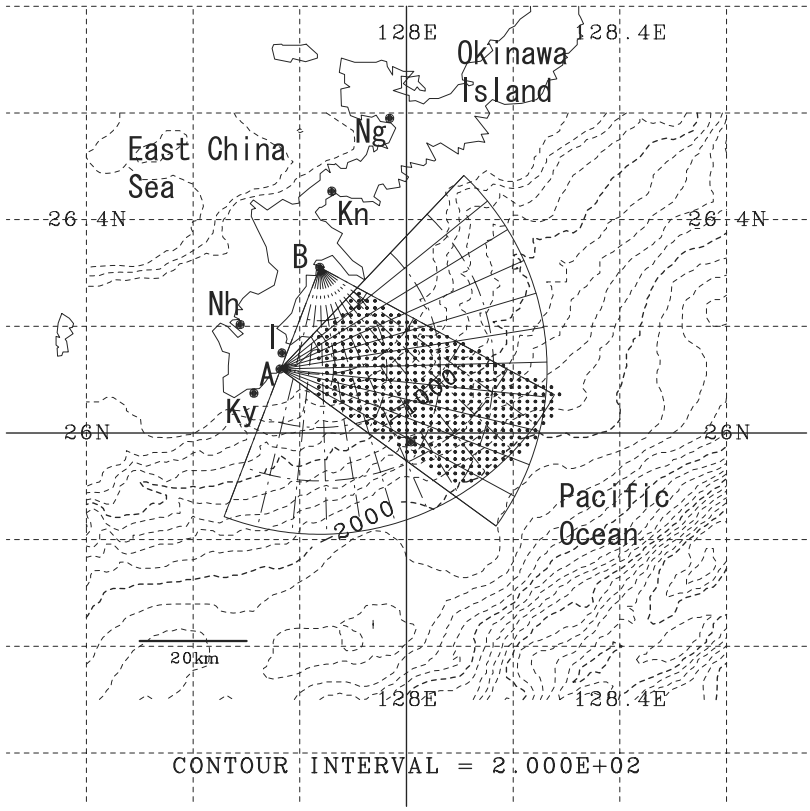

Figure 2. Map of the observation area: A and B, locations of the HF ocean radars; Ky, Kyan (wave station); Ng, Nago; Kn, Kin; I, Itokazu; Nh, Naha (meteorological station); and P, current meter observation.

Time) means average winds from 1150 to 1200 JST. An hourly or 2 hourly mean wind is defined in a similar way.

[20] The resolution of the wind speed was 1 ms^{-1} and the resolution of wind direction was 22.5° (16 directions). Furthermore, hourly significant wave heights (H_s) and wave periods (T_s) at location Ky (Kyan, 26° 4′N, 127° 43′E) were also supplied by JMA. The acoustic wave sensor was used for the measurement at a water depth of 51 m and 1370 m off the coast.

[21] A current meter was deployed at location P shown in Figure 2 (Payao, 25° 59′N, 128° 0.5′E) from the Okinawa Prefectural Fisheries Experiment Station. The water depth at deployment was 4 m. HF ocean radar-derived currents were compared with currents measured using the current meter at Payao, and the results were in good agreement. The correlations were greater than 0.85, and the root mean square difference between them was about 10 cm s^{-1} for both east-west and north-south components [*Hisaki et al.*, 2001].

3. Spatial and Temporal Variability

[22] Figure 3 shows an example of short-wave directions, spread parameters, and ocean currents. A wind at Itokazu is also presented. To reduce variability further, the radar-estimated data were spatially running-averaged at 9 points. The mean short-wave directions is the direction of the mean vector of unit vectors of short-wave directions. Short-wave data with large error ($\langle \Delta\theta_m^2 \rangle^{1/2} > 15°$, $\langle \Delta s^2 \rangle^{1/2} > 0.5$, section 2.2) are removed. The wind and short-wave directions were northwest ward, while directions of ocean currents were different from that of the wind.

[23] Figure 4 shows time series of significant wave heights, wave periods at Kyan (Ky in Figure 2) and hourly mean winds at Itokazu (I in Figure 2). The wave heights were higher on 21 and 25 April. Wind speeds were relatively high, and atmospheric fronts passed over the HF radar observation area during these days. Most of the wind directions were northwestward or northward. In particular, the northward or northwestward winds were relatively steady from 7 May to 16 May.

[24] Figure 5a shows time series of 2 hourly mean wind directions at Itokazu (I in Figure 2, θ_w), radar-estimated short-wave directions at the closest grid point to Itokazu (θ_m), and the difference between them ($\theta_w - \theta_m$). Figure 5b is a scatter diagram between wind directions and short-wave directions.The closest grid point to Itokazu is about 10 km from Itokazu. Wind directions and short-wave directions are plotted with different symbols according to the value of $|\theta_w(t) - \theta_w(t - \Delta t)|$, where t is the time and Δt = 2 hours.

[25] The number of samples for the comparison was 226. The comparison is summarized in Figure 5. The agreement is fairly good. The correlation was about 0.96, and the root mean square difference from the linear regression line was about 31° The difference between wind directions (I in Figure 2) and radar-estimated short-wave directions are due to horizontal variations of winds and a time lag of short-wave response to a sudden wind shift.

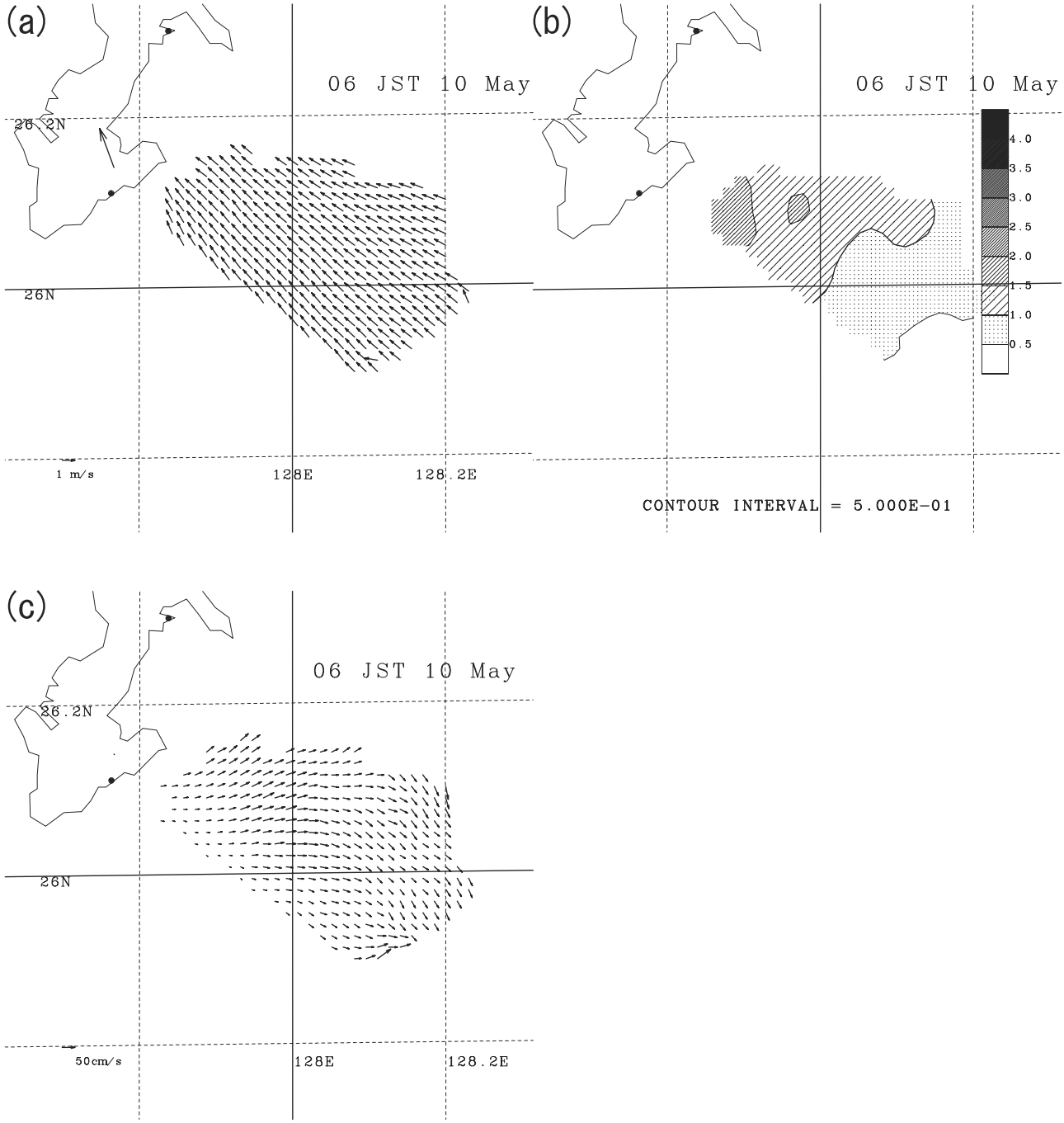

Figure 3. Example of (a) short-wave directions, (b) spread parameters, and (c) ocean currents (6 JST 10 May 1998). The magnitudes of short-wave directions are scaled to 1 m/s.

[26] For example, there were abrupt shifts in wind directions at 14 JST 17 April, 12 JST 25 April, and 0 JST 4 May, when discrepancies between wind directions and short-wave directions were large. The case of 25 April is explained in section 4.

[27] Many of the out liers in Figure 5b are related to shifts in wind directions, although there are exceptions. The time of the exceptions (out liers plotted with black circles in Figure 5b) are 22 JST 17 April (θ_w = 22°, θ_m = 159°), 6 JST 20 April (θ_w = −48°, θ_m =49°) and 14 JST 25 April (θ_w = −58°, θ_m = 84°). As shown later, spatial variabilities of short-wave directions were large in these periods.

[28] Figure 6 shows horizontal distributions of mean values and standard deviations of short-wave directions. The author presented short-wave properties, where wave data were collected more than 75% of the time. The mean short-wave directions were mostly northwestward. The mean spread parameters were large near the coast and small off the coast. Standard deviations of both short-wave directions and spread parameters were small near the coast and large off the coast.

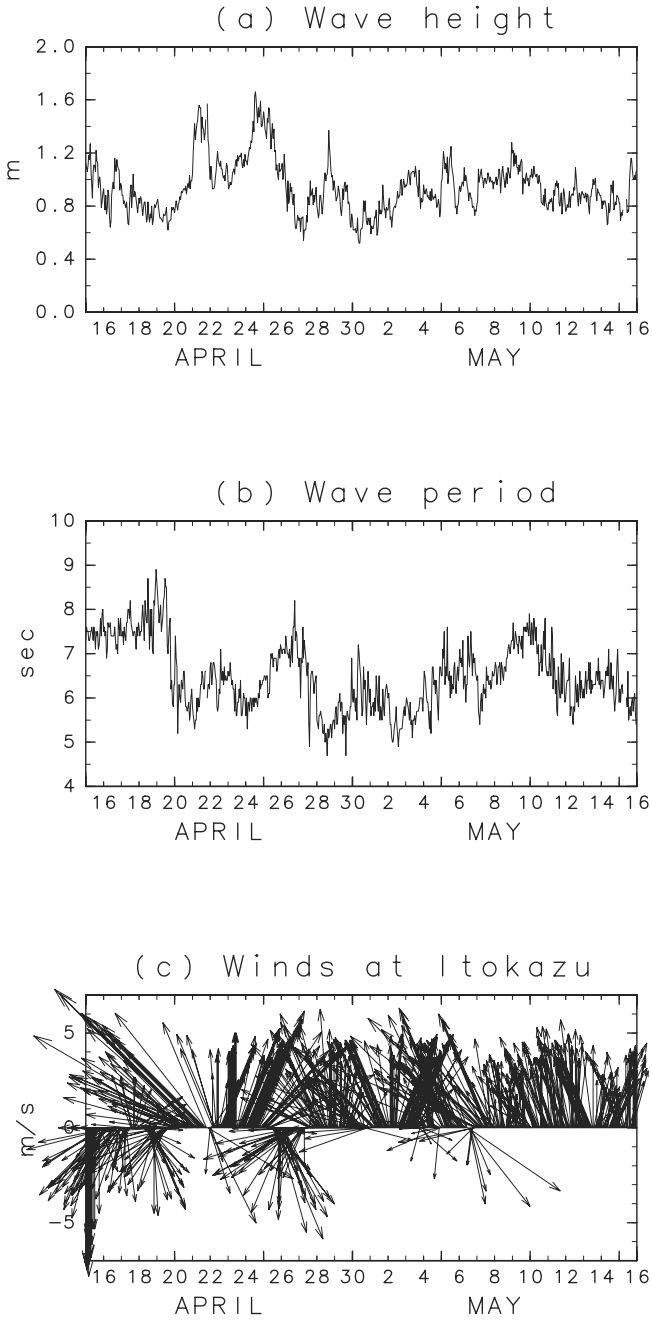

Figure 4. Time series of significant wave heights, wave periods at Kyan (Ky in Figure 2), and hourly mean winds at Itokazu (I in Figure 2).

[29] The wave refraction over the bottom topography is not so significant, because the water depth in most of the HF radar observation area is deep even near the coast (Figure 2). One possible explanation is that winds near the coast are controlled by topography. As a result, wave directional distributions are narrower near the coast, and the mean value of the spread parameter is large. On the other hand, surface winds are variable off the coast, and the angular spread is broad. Another explanation is that the value of f_B/f_m (f_m is a peak wave frequency) is large in the offshore area. In general, the wave angular spread becomes broader with higher normalized frequencies [e.g., *Mitsuyasu et al.*, 1975], and waves develop in the offshore area.

[30] A plausible reason as to why the peak wave period is longer offshore is that the sea surface wind speed is stronger offshore. However, we do not have wind or wave data from ocean buoys in our study region. The difference between offshore and nearshore waves should be investigated using data obtained from ocean buoys. A large mean spread parameter corresponds to a small standard deviation.

[31] Figure 7 shows time series of area-averaged radar-estimated short-wave directions, area-averaged spread parameters and their standard deviations, and wind directions at Itokazu. Standard deviations of short-wave directions and spread parameters indicate horizontal variabilities of wave fields. The overall average of spread parameters was 1.19. The horizontal variations of short-wave directions

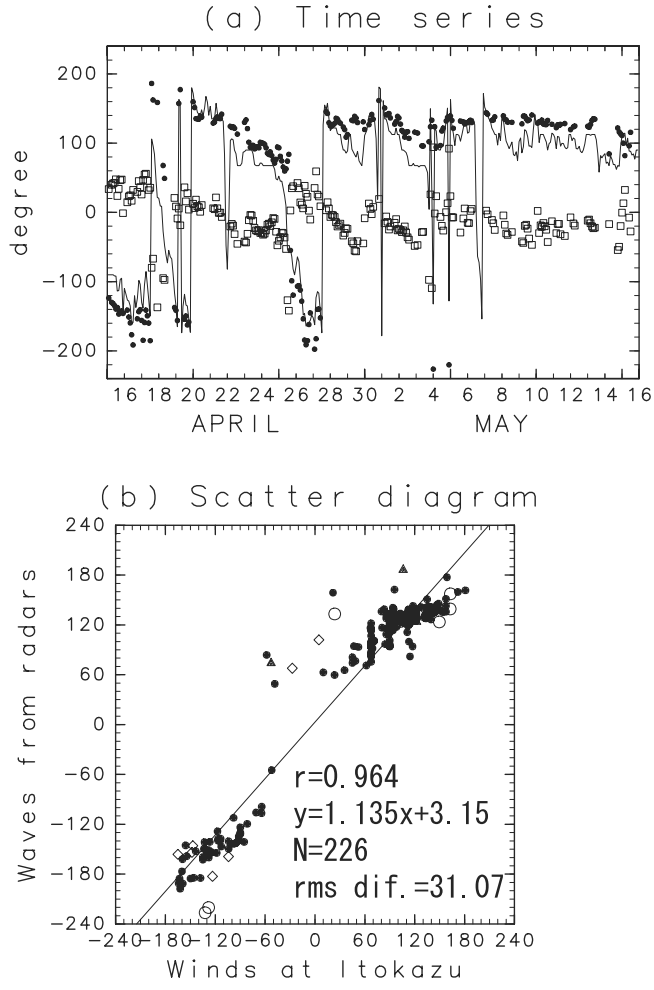

Figure 5. (a) Time series of 2 hourly mean wind directions with respect to the eastward direction (counterclockwise is positive)at Itokazu (θ_w, solid line), radar-estimated short-wave directions at the closest grid point to Itokazu (θ_m, solid circle), and difference between them ($\theta_w - \theta_m$, open square) and (b) scatter diagram between them. Solid circles denote $|\theta_w(t) - \theta_w(t - \Delta t)| \leq 30°$, open diamonds denote $30° < |\theta_w(t) - \theta_w(t - \Delta t)| \leq 60°$, solid triangles denote $60° < |\theta_w(t) - \theta_w(t - \Delta t)| \leq 90°$, and open circles denote $60° < |\theta_w(t) - \theta_w(t - \Delta t)| > 90°$.

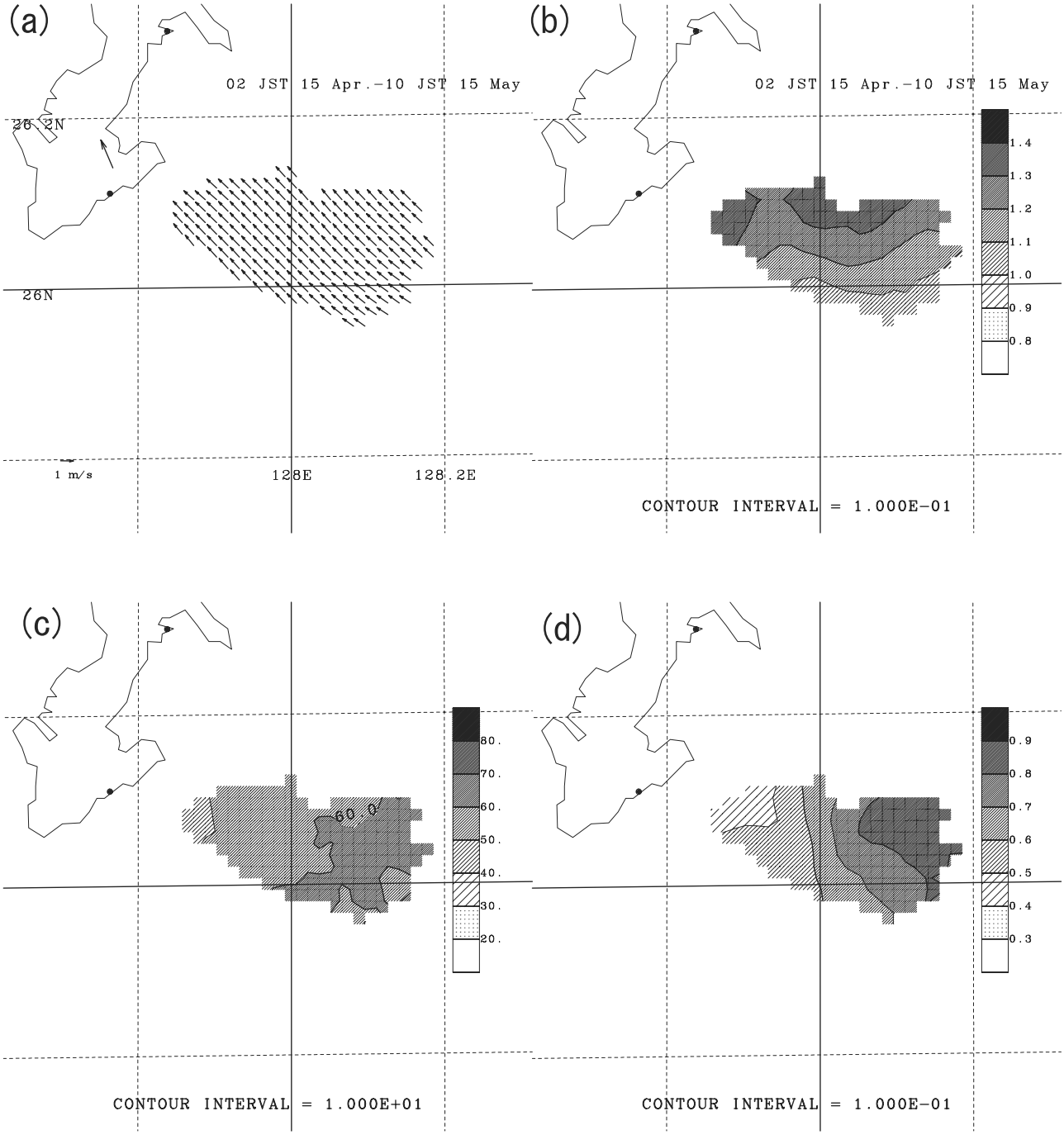

Figure 6. Mean values and standard deviations of short-wave directions and spread parameters during the HF radar observation period (from 2 JST 15 April to 10 JST 15 May 1998): (a) Mean short-wave directions, (b) mean spread parameters, (c) standard deviation of short-wave directions, and (d) standard deviation of spread parameters.

were large when the winds or short-waves significantly changed their directions, for examples, at 2 JST 18 April, 0 JST 22 April, 18 JST 30 April and 22 JST 3 May. On the other hand, values of spread parameters were small during these periods due to complicated wave directional properties such as bimodal distributions associated with a large change in wind direction.

[32] Because the author does not have sea surface wind data, he cannot compare radar-estimated area-averaged spread parameters s with empirical formulas of the spread parameters [e.g., *Mitsuyasu et al.*, 1975; *Hasselmann et al.*, 1980; *Donelan et al.*, 1985]. The author compared spread parameters s with empirical formulas using wind data at Itokazu for the whole HF ocean radar observation period, but could not find a relationship.

[33] The sea surface wind is stronger than the land surface wind because the sea surface is smoother than the land surface. The elevation of Itokazu is 186 m from the sea

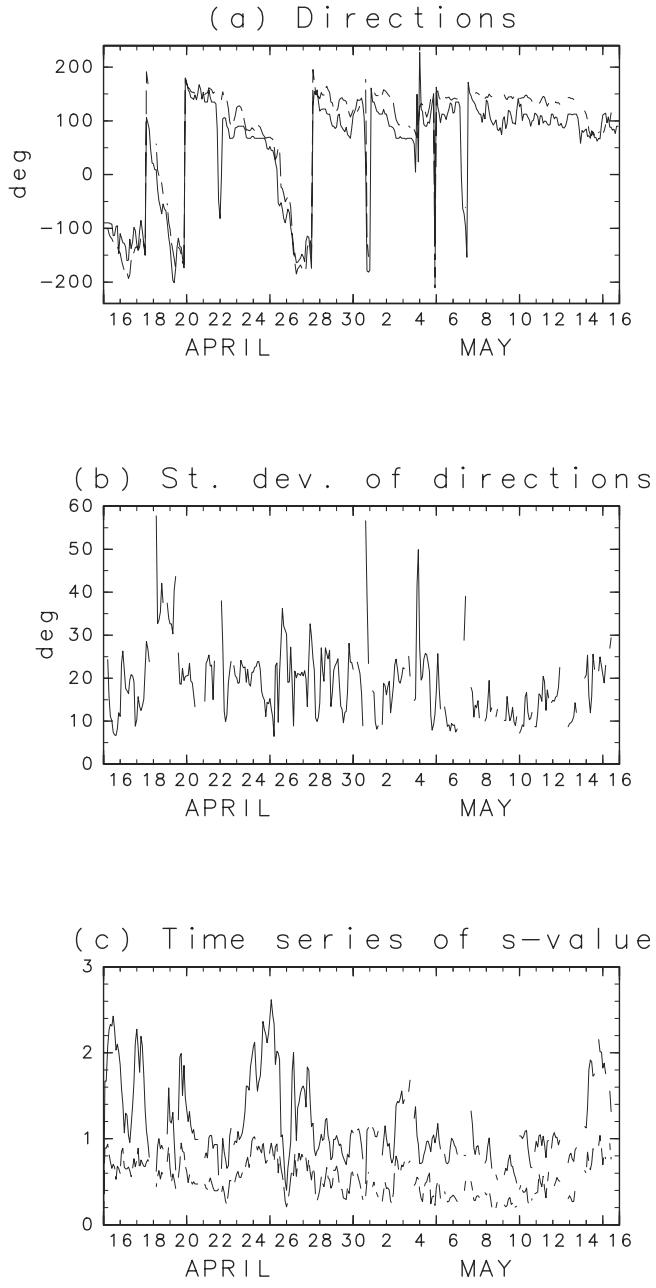

Figure 7. Time series of (a) area-averaged radar-estimated short-wave directions (dashed line) and wind directions with respect to the eastward direction (counterclockwise is positive)at Itokazu (solid line), (b) standard deviations of short-wave directions, and (c) area-averaged spread parameters (solid line) and standard deviations of spread parameters (dashed line).

surface, therefore, the conversion from wind speeds at Itokazu to sea surface wind speeds at 10 m height is uncertain.

[34] Figure 8 shows a scatter diagram between $\log_{10}(f_B/f_m)$ and $\log_{10} s$ from 7 May to 15 May, where f_m is the peak wave frequency estimated from $f_m = 1/(1.05T_s)$. As noted previously, winds are relatively stationary during this period.

[35] The correlation was −0.36, which is significant at the 99% confidence level. The negative correlation is qualitatively consistent with results of previous studies [e.g., *Mitsuyasu et al.*, 1975; *Hasselmann et al.*, 1980; *Donelan et al.*, 1985], although normalized frequencies (f_B/f_m) are higher than those in previous studies. In Donelan's formula [*Donelan et al.*, 1985], the angular spread is independent of the frequency for $f/f_m > 1.6$ ($\log_{10}(f/f_m) > 0.2$), however, this result shows that the angular spread becomes broader with higher frequency. There was no correlation between $\log_{10}(f_B/f_m)$ and $\log_{10} s$ for the whole HF ocean radar observation period, because the wind field was not stationary during that period.

[36] The author defines the index of wind unsteadiness at time t as

$$W_s = W_s(t) = \frac{|\mathbf{u}_w(t) - \mathbf{u}_w(t - \Delta t)|}{|\mathbf{u}_w(t)|}, \tag{13}$$

where $\mathbf{u}_w(t)$ is a 2 hourly mean wind vector at Itokazu and Δt = 2 hours. Different symbols are plotted in Figure 8 according to the range of the index W_s. The number of data points for each range of W_s is 20 for $W_s \leq 0.15$, 29 for $0.15 < W_s \leq 0.3$, 15 for $0.3 < W_s \leq 0.45$, and 12 for $W_s > 0.45$.

[37] We cannot see a clear relationship between the index W_s and the $\log_{10}(f_B/f_m)-\log_{10} s$ relation. However, data points for $W_s \leq 0.15$ (black circles) seem to exist in the vicinity of the lower boundary of the scatter diagram, except at one point ($\log_{10}(f_B/f_m) = 0.51$ and $\log_{10} s = 0.25$ at 4 JST 14 May), which suggests that there is a coherent

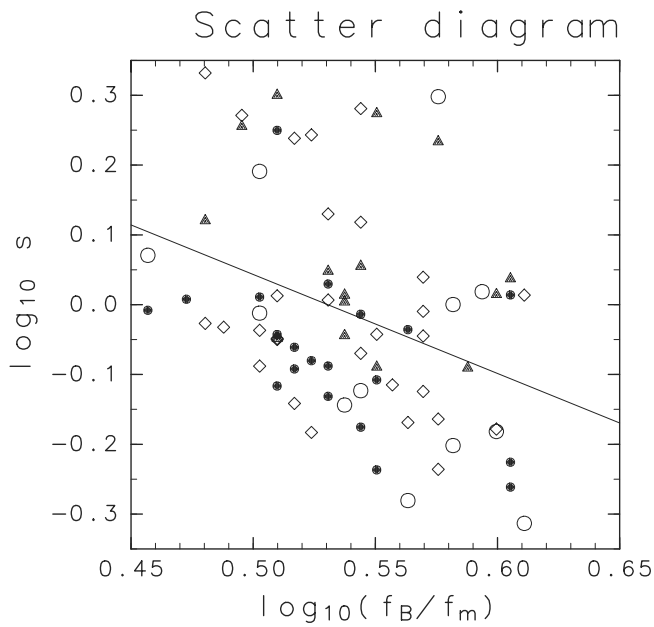

Figure 8. Scatter diagram between $\log_{10}(f_B/f_m)$ and $\log_{10} s$ from 7 May to 15 May, where f_m is the peak wave frequency. Solid circles denote $W_s \leq 0.15$ (W_s is defined in equation (13)), open diamonds denote $0.15 < W_s \leq 0.3$, solid triangles denote $0.3 < W_s \leq 0.45$, and open circles denote $W_s > 0.45$.

relationship between s and f_B/f_m in the case of a steady wind.

4. Atmospheric Front

[38] Figure 9 shows JMA weather charts. The weather charts are drawn based on the meteorological data from land stations shown in Figure 2, and ship data. Examples of the location of ships in the vicinity of the HF radar observation area, data from which were used to draw Figure 9a, are (24.8°N, 130.3°E), (29.9°N, 133.1°E), (28.3°N, 126.6°E), and (24.7°N, 133.1°E).

[39] An atmospheric front passed over the HF ocean observation area from 9 JST to 15 JST 25 April, and propagated eastward. Figure 10 shows time series of winds on 25 April. Wind directions changed from northeastward to southeastward at 9 JST in Nago, Kin, Naha and Itokazu, which was associated with the passage of the atmospheric front. Furthermore, winds changed their directions from northeastward to southeastward once at 4 or 5 JST in Nago and Kin, which are north of the HF ocean radar observation area.

[40] Figure 11 shows radar-estimated short-wave directions on 25 April. The wind direction and short-wave directions were northeastward until 6 JST (Figure 11d). The short-wave directions in the northeastern part of the HF ocean radar observation area changed to southeastward. However, the short-wave directions returned again to northeastward again on 12 JST (Figure 11g). The wind direction changed to southeastward at 10 JST, while short-wave directions were mostly northeastward at this time. The short-wave directions changed to southeastward at 16 JST (Figure 11i), although they were still northeastward in the southeastern part. The short-wave directions in the southeastern part were northeastward at 18 and 20 JST. They changed to southeastward at 22 JST.

[41] The time scale of the response of ocean waves with frequency f_B to veering winds is

$$t_c = \frac{1}{2\pi b f_B} \tag{14}$$

for $U/v_p < 2$, where $b \simeq 2 \times 10^{-5}$, U is the wind speed at 10 m height, and v_p (=3.09 m/s) is the phase speed [*Hasselmann et al.*, 1980]. Therefore, the time scale is $t_c \simeq 4.4$ hours. This is consistent with the difference in the time of the change in winds and short-wave directions, although there is a possibility that from 16 to 20 JST the front stayed between the HF ocean observation area and Itokazu.

[42] The explanation for the appearance of southwestward short-waves only in the northeastern part at 8 and 10 JST (Figures 11e and 11f) is not entirely clear. One is that the frontal structure is wavy, and these southeastward short waves correspond to the southeastward winds at 4 or 5 JST in Nago and Kin (Figures 10a and 10b). Thus, we can see detailed frontal structures which cannot be detected by a weather chart.

5. Oceanic Front

5.1. Convergent Zone

[43] A prominent convergent zone often appeared in the HF ocean radar observation area. In particular, the maximum value of convergence ($-\nabla_H \cdot \mathbf{u}$, $\mathbf{u} = (u, v)$: two-dimensional current vector) for daily averaged currents was about 10×10^{-5} s^{-1} on 17 April 1998 [*Hisaki et al.*, 2001]. Figure 12a shows a horizontal distribution of short-wave directions, and Figure 12b shows an example of the current field during the period. We can see a strong convergent zone along 26°N latitude.

[44] General features of the current fields on 17 April were similar to those in Figure 12b: in the coastal area (i.e., west of 128°E), the currents were southward or southwestward; in the southern part of the offshore area (i.e., east of 128°E and south of 26°N), the currents were southeastward; in the northern part of the offshore area, the currents were southward. The wind direction and short-wave directions were southward or southwestward.

[45] It was found, from the analysis of SST (sea surface temperature) and altimetric data, that the convergent zone was associated with the front of a mesoscale eddy [*Hisaki et al.*, 2001]. Figure 12c shows an example of spread parameters during the period. The spreading parameter was large in the vicinity of the convergent front. The author investigated whether or not such a convergence could contribute to the spatial variability of short-wave directional properties, by calculating spread parameters s using the simplified model based on the wave action conservation law.

[46] The wave action conservation law is written as

$$\frac{\partial N}{\partial t} + (\mathbf{u} + \mathbf{C}_g) \cdot \frac{\partial N}{\partial \mathbf{x}} + [-\mathbf{k} \cdot \nabla_H \mathbf{u} - \mathbf{k} \times (\nabla_H \times \mathbf{u})] \cdot \left(\frac{\partial N}{\partial \mathbf{k}}\right) = Q, \tag{15}$$

where t is the time, $N = N(\mathbf{k}, \mathbf{x}, t) = S(\mathbf{k}, \mathbf{x}, t)/\omega$ is the action spectral density, $\omega = (gk)^{1/2}$ is the intrinsic radian frequency, $\mathbf{C}_g = \partial\omega/\partial\mathbf{k}$ is the group velocity vector, Q is the source function, and $S(\mathbf{k}, \mathbf{x}, t)$ is the wave spectrum.

5.2. Simplified Model

[47] To explore the effect of the convergence on wave directional distributions, the author simplified equation (15) by assuming a steady state ($\partial N/\partial t = 0$), a homogeneous field in the y-direction ($\partial/\partial y = 0$), and no wind input ($Q = 0$). Furthermore, the author approximated equation (15) as $\partial N/\partial k \simeq \partial N_0/\partial k$ and $\partial N/\partial\theta \simeq \partial N_0/\partial\theta$, where N_0 is the equilibrium action density. Thus, equation (15) is simplified and approximated as

$$C_x \frac{\partial N}{\partial x} + D_v \frac{\partial N_0}{\partial(\log k)} + D_r \frac{\partial N_0}{\partial\theta} = 0, \tag{16}$$

where

$$C_x = \frac{g}{2\omega}\cos\theta + u, \tag{17}$$

$$D_v = -\left(\cos^2\theta \frac{\partial u}{\partial x} + \cos\theta \sin\theta \frac{\partial v}{\partial x}\right), \tag{18}$$

and

$$D_r = \cos\theta \sin\theta \frac{\partial u}{\partial x} + \sin^2\theta \frac{\partial v}{\partial x}. \tag{19}$$

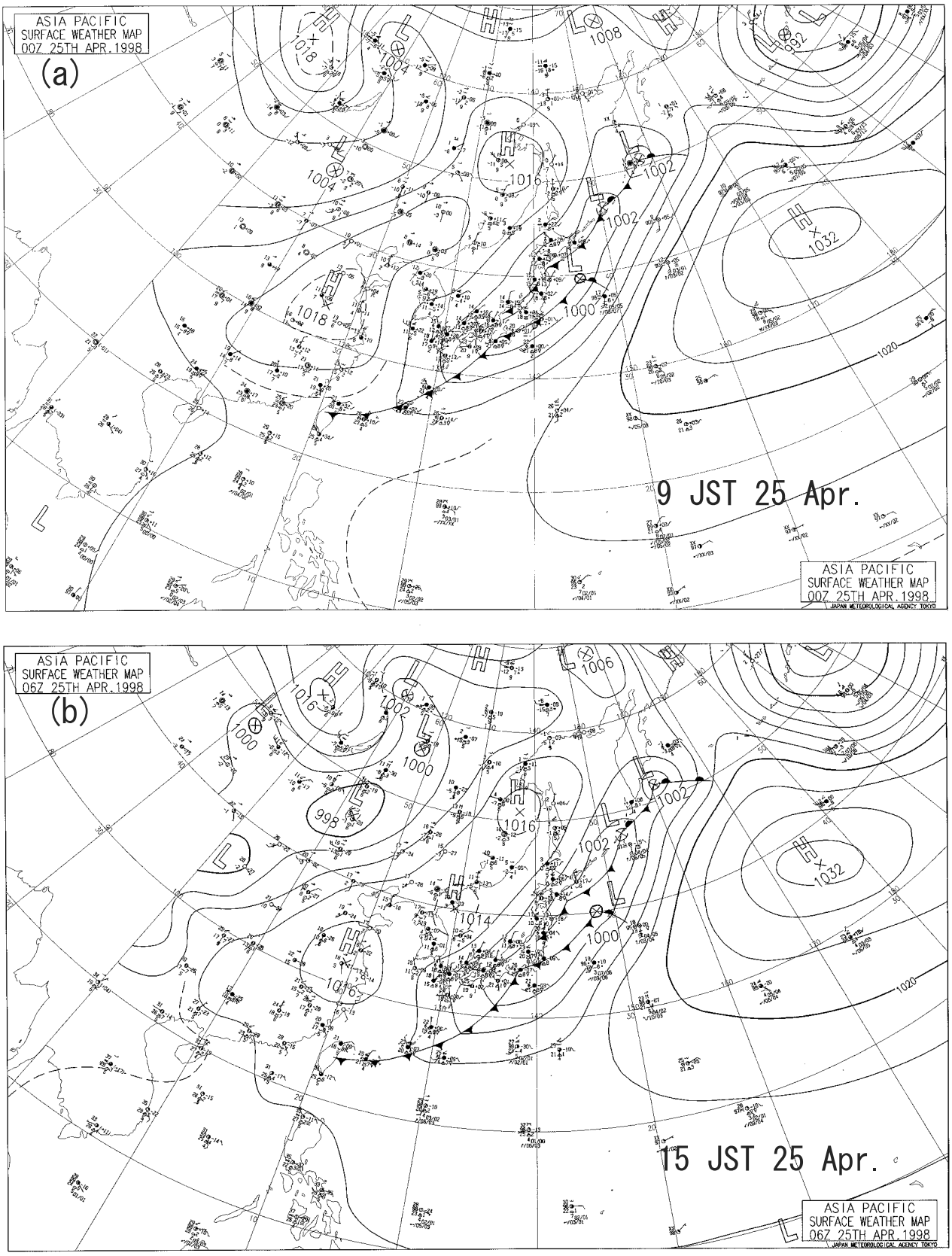

Figure 9. JMA weather chart (provided by JMA): (a) 9 JST 25 April 1998 and (b) 15 JST 25 April 1998.

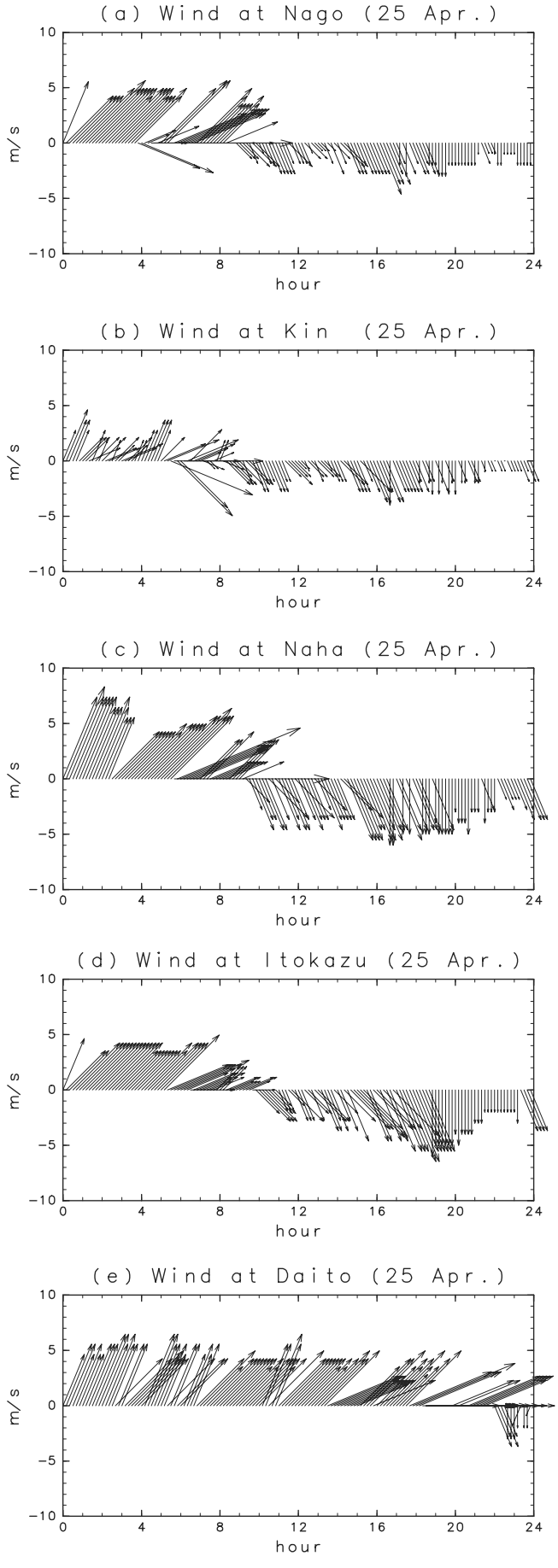

Figure 10. (opposite) Time series of winds on 25 April 1998 at five stations: (a) Nago, (b) Kin, (c) Naha, (d) Itokazu, and (e) South-Daito island.

The boundary condition is $N = N_0$ at $x = -L$. In this example, the current velocity is expressed as

$$\begin{aligned} &u = d_u x + u_b \ (-L \le x \le L), \\ &u = const. \ (x < -L, \text{or } x > L), \\ &v = 0, \end{aligned} \tag{20}$$

and equation (16) is modified to

$$N = N_0 - \frac{\partial N_0}{\partial \log k} \int_{-L}^{x} \frac{D_v}{C_x} dx - \frac{\partial N_0}{\partial \theta} \int_{-L}^{x} \frac{D_r}{C_x} dx, \tag{21}$$

where

$$\int_{-L}^{x} \frac{D_v}{C_x} dx = -\cos^2\theta \log \frac{|d_u x + u_b + \frac{g}{2\omega}\cos\theta|}{|d_u L - u_b - \frac{g}{2\omega}\cos\theta|}, \tag{22}$$

$$\int_{-L}^{x} \frac{D_r}{C_v} dx = -\cos\theta \sin\theta \log \frac{|d_u x + u_b + \frac{g}{2\omega}\cos\theta|}{|d_u L - u_b - \frac{g}{2\omega}\cos\theta|}. \tag{23}$$

[48] The wave spectrum at the boundary (ωN_0) is of the Pierson-Moskowitz form and $s = 2$ for the directional distribution expressed by equation (3). The author calculated $N = N(2k_0, \theta, x)$ from equations (21), (22), and (23), fitted the model function (equation (3)) to $N(2k_0, \theta, x)$, and estimated $\theta_m = \theta_{ma}$ and $s = s_a$ by the least squares method. Figure 13 shows the results of the calculation of $\theta_{ma} - \theta_m$ and s_a for $N(2k_0, \theta, x)$ as a function of position (x) and mean wave direction at $x = -L$ (θ_m).

[49] The parameters used are $d_u = -10^{-5} s^{-1}$, $u_b = 0$, $L =$ 12 km, and $f_m = 0.15$ Hz. The wave directional distribution is the narrowest at $\theta_m = 0°$ is the broadest at $\theta_m = 180°$. The main incident wave comes in from a positive x for $90° < \theta_m \le 180°$ The wave directional distribution becomes narrower farther down wave(downwind) from the position of incidence, except at $90° < \theta_m < 120°$ which is due to refraction by currents. The wave refraction direction ($\theta_{ma} - \theta_m$) is the largest when the current direction is the crosswind direction. This result indicates that the wave directional distribution is narrow in the vicinity of the convergent front.

6. Concluding Remarks

[50] Although the wave frequency is limited to 0.505 Hz, it is easy to estimate short-wave directional properties from HF ocean radar data. In general, it is difficult to estimate a directional spectrum at such a high frequency by a conventional method such as one that uses data from a pitch-roll buoy. The author estimated short-wave directional properties, and he described their spatial and temporal variabilities. The agreement between wind directions and short-wave directions was good, which indicates that short-waves respond to winds. The values of spread parameters were related to the variabilities of short-wave directions or winds. For example, the angular spread was broader in the offshore area, which was explained by the large variability of wind

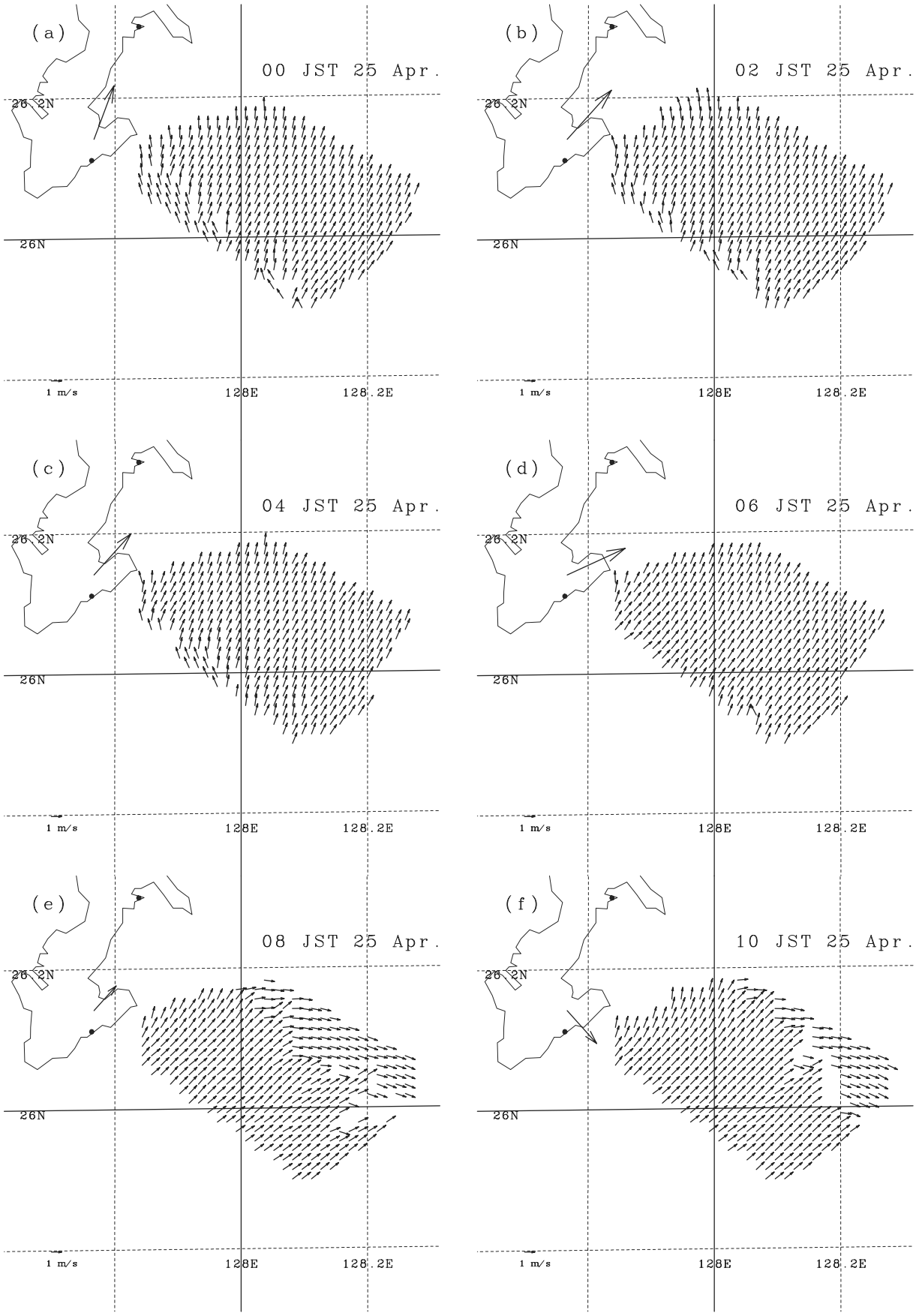

Figure 11. Radar-estimated short-wave directions on 25 April 1998: (a) 0 JST, (b) 2 JST, (c) 4 JST, (d) 6 JST, (e) 8 JST, (f) 10 JST,(g) 12 JST, (h) 14 JST, (i) 16 JST, (j) 18 JST, (k) 20 JST, and (l) 22 JST.

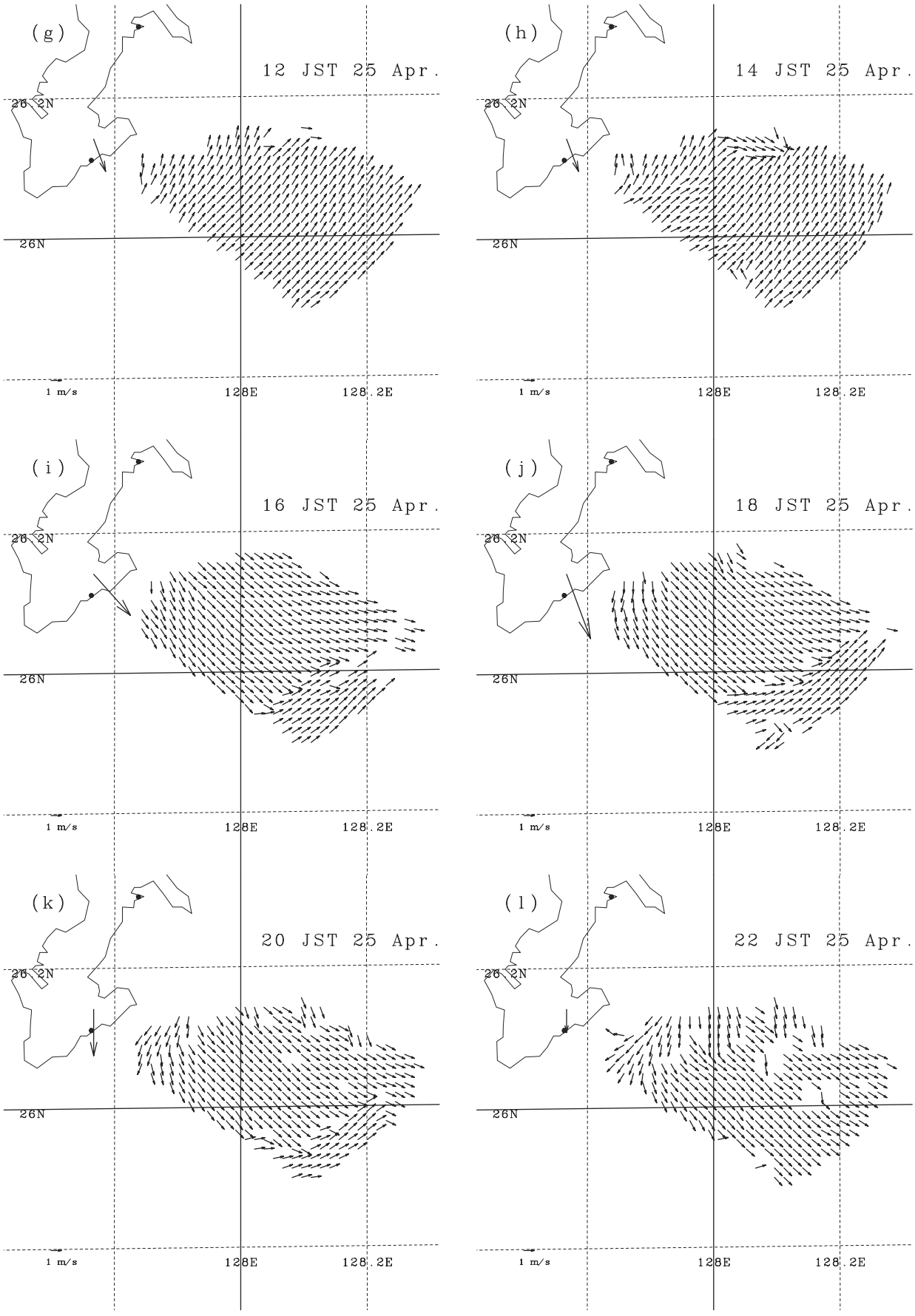

Figure 11. (continued)

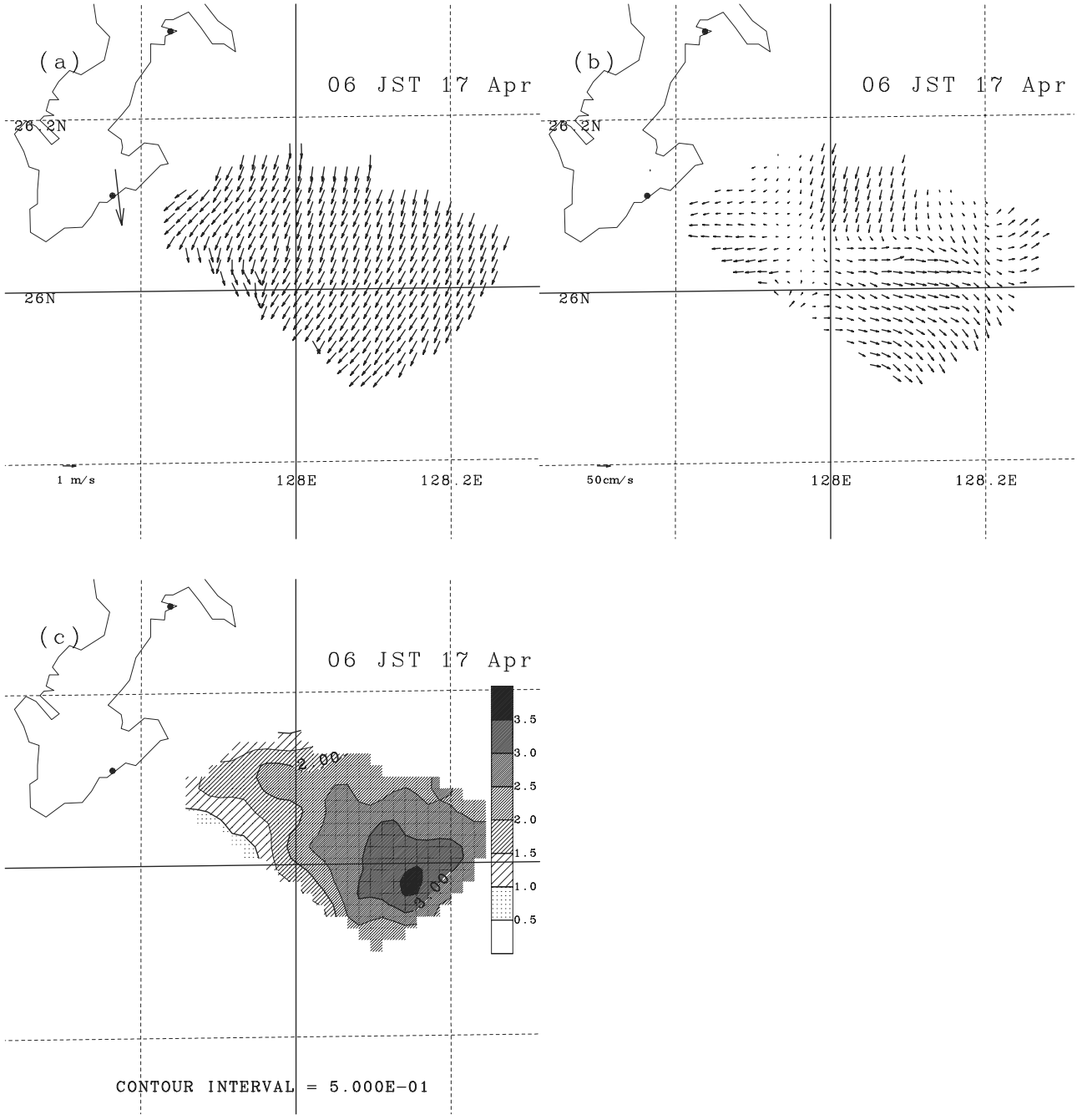

Figure 12. (a) Short-wave directions, (b) surface current fields, and (c) spread parameters at 6 JST 17 April 1998 estimated using data from HF ocean radar.

direction in the offshore area. Furthermore, the angular broadening was related to the change of wind direction. Under steady wind conditions, the spread parameter becomes small when the normalized frequency f_B/f_m increases, which is consistent with the results of previous studies, although this was not verified in the range of such a high normalized frequency in those studies.

[51] The author described the short-wave direction field when an atmospheric front passed over the HF ocean radar observation area. The passage of the atmospheric front was reflected in the radar-estimated short-wave fields. However, there was a time lag between a change in wind direction and a change in short-wave direction, which is consistent with the result of a previous study [*Hasselmann et al.*, 1980]. Furthermore, it is suggested that the frontal structure is wavy, which cannot be detected by a weather chart.

[52] There was a prominent convergence associated with the front of a mesoscale eddy. A narrow directional spread parameter was obtained using data from HF ocean radars. The author investigated whether or not such a current field could account for the horizontal distribution of spread parameters, using a simplified model. This model is based on the conservation of wave action density with no wind input. The model is in the steady state and one-dimensional.

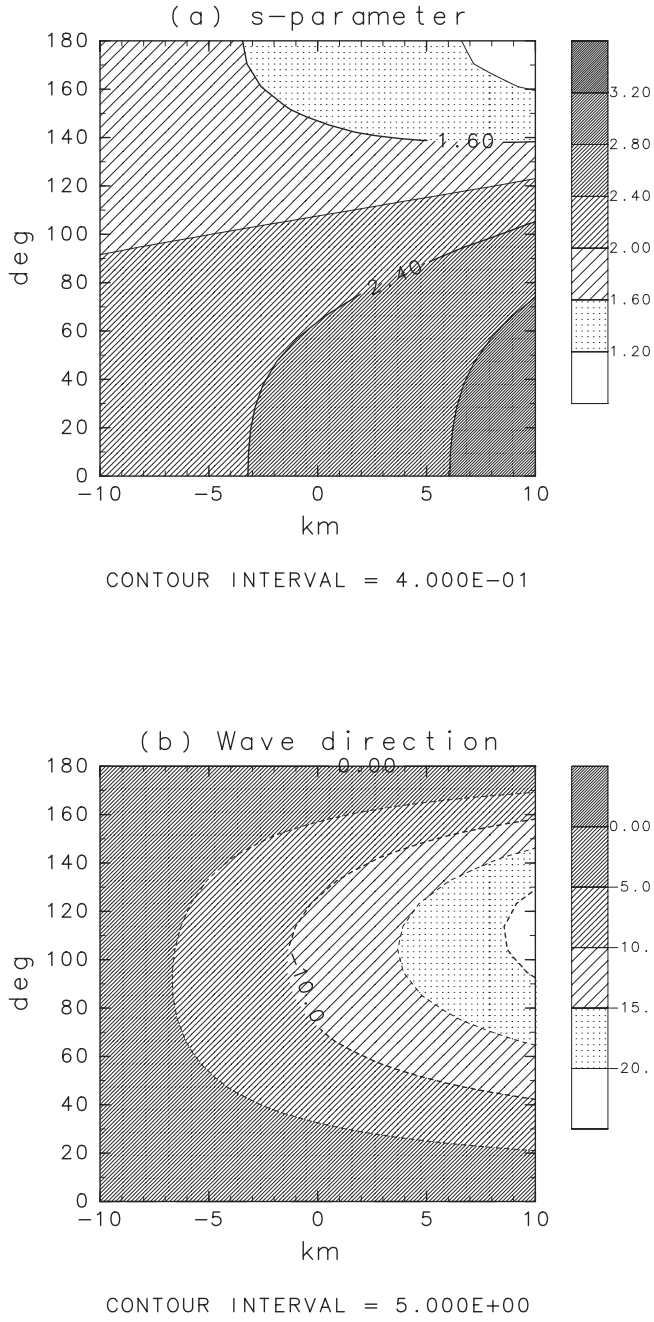

Figure 13. Wave directional distribution at the Bragg wave number refracted by convergent currents: (a) Spread parameter (s_a), and (b) refracted mean wave direction with respect to the mean wave direction at $x = -L$ ($\theta_{ma} - \theta_m$, unit = deg).

The narrow directional spread parameter was reproduced using the model. This result shows that wave refraction associated with a frontal convergent zone is important in the spatial variability of short-wave directional properties. The application of the realistic model to the observed currents is the next subject of study.

[53] The unimodal model function of the short-wave directional distribution, equation (3),was assumed to estimate the short-wave directional distribution. However, recent observations of surface waves revealed that the wave directional distribution was bimodal rather than unimodal under fetch-limited conditions [e.g., *Young et al.*, 1995; *Ewans*, 1998]. The directional bimodality will be investigated using HF ocean radar.

[54] **Acknowledgments.** The author acknowledges the anonymous reviewers for their insightful comments which contributed to the improvement of the manuscript. The author acknowledges staff of Okinawa Radio Observatory, Communications Research Laboratory for providing Doppler spectrum data from HF ocean radar. The author acknowledges Japan Meteorological Agency for providing the meteorological data and wave data. The GFD-DENNOU Library (http://dennou.gaia.h.kyoto-u.ac.jp/arch/dcl/) was used in drawing the figures.

References

Barrick, D. E., First-order theory and analysis of MF/HF/VHF scatter from the sea, *IEEE Trans. Antennas Propag.*, *20*, 2–10, 1972.

Barrick, D. E., Extraction of wave parameters from measured HF sea-echo Doppler spectra, *Radio Sci.*, *12*, 415–424, 1977.

Barrick, D. E., Accuracy of parameter extraction from sample-averaged sea-echo Doppler spectra, *IEEE Trans. Antennas Propag.*, *28*, 10–11, 1980.

Donelan, M. A., J. Hamilton, and W. H. Hui, Directional spectra of wind-generated waves, *Philos. Trans. R. Soc. London., Ser. A*, *315*, 509–562, 1985.

Ewans, K. C., Observations of the directional spectrum of fetch-limited waves, *J. Phys. Oceanogr.*, *28*, 495–512, 1998.

Forget, P., P. Broche, J. C. Maistre, and A. Fontanel, Sea state frequency features observed by ground wave HF Doppler radar, *Radio Sci.*, *16*, 917–925, 1981.

Harlan, J. A., and T. M. Georges, An empirical relation between ocean-surface wind direction and the Bragg line ratio of HF radar sea echo spectra, *J. Geophys. Res.*, *99*, 7971–7978, 1994.

Hasselmann, D. E., M. Dunckel, and J. A. Ewing, Directional wave spectra observed during JOWSWAP 1973, *J. Phys. Oceanogr.*, *10*, 1264–1280, 1980.

Heron, M. L., Directional spreading of short wavelength fetch-limited wind waves, *J. Phys. Oceanogr.*, *17*, 281–285, 1987.

Hisaki, Y., Nonlinear inversion of the integral equation to estimate ocean wave spectra from HF radar, *Radio Sci.*, *31*, 25–39, 1996.

Hisaki, Y., Correction of amplitudes of Bragg lines in the sea echo Doppler spectrum of an ocean radar, *J. Atmos. Oceanic Technol.*, *16*, 1416–1433, 1999.

Hisaki, Y., and M. Tokuda, VHF and HF sea-echo Doppler spectrum for a finite illuminated area, *Radio Sci.*, *3*, 425–440, 2001.

Hisaki, Y., W. Fujiie, T. Tokeshi, K. Sato, and S. Fujii, Surface current variability east of Okinawa Island obtained from remotely sensed and in-situ observational data, *J. Geophys. Res.*, *106*, 31,057–31,073, 2001.

Masson, D., A case study of wave-current interaction in a strong tidal current, *J. Phys. Oceanogr.*, *26*, 359–372, 1996.

Mitsuyasu, A., F. Tasai, T. Suhara, S. Mizuno, M. Ohkusu, T. Honda, and K. Rikiishi, Observations of the directional spectrum of ocean waves using a cloverleaf buoy, *J. Phys. Oceanogr.*, *5*, 750–760, 1975.

Wang, D. W., A. K. Liu, C. Y. Peng, and E. A. Meindl, Wave-current interaction near the Gulf Stream during the Surface Wave Dynamics Experiment, *J. Geophys. Res.*, *99*, 5065–5079, 1994.

Wyatt, L. R., L. J. Ledgard, and C. W. Anderson, Maximum-likelihood estimation of the directional distribution of 0.53-Hz ocean waves, *J. Atmos. Oceanic. Technol.*, *14*, 591–603, 1997.

Young, I. R., L. A. Verhagen, and M. L. Banner, A note on the bimodal directional spreading of fetch-limited wind waves, *J. Geophys. Res.*, *100*, 773–778, 1995.

Y. Hisaki, Department of Physics and Earth Sciences, Faculty of Science, University of the Ryukyus 1 Aza-Senbaru, Nishihara-cho, Nakagami-gun, Okinawa 903-0213, Japan. (hisaki@sci.u-ryukyu.ac.jp)